PCCP

Dissociative photodetachment dynamics of the oxalate monoanion

SCHOLARONE™
Manuscripts

Journal Name

Dissociative photodetachment dynamics of the oxalate monoanion

J. A. Gibbard, [a] E. Castracane, [a] A. J. Shin, [a] and R. E. Continetti [a]

The dissociative photodetachment (DPD) dynamics of the oxalate monoanion are studied using photoelectron-photofragment coincidence (PPC) spectroscopy. Following photodetachment of $C_2O_4H^-$ at 4.66 eV HOCO $+ CO_2$ products are observed, indicating the facile decarboxylation of the radical driven by the thermodynamic stability of CO_2. No evidence is seen for photodetachment to stable C_2O_4H or ionic photodissociation to produce HOCO$^-$. Calculations indicate the stabilizing presence of an intramolecular hydrogen bond in the anion via the formation of a strained five-membered ring. No intramolecular hydrogen bond is predicted in the radical due to the lower charge density on the oxygen atom. The PPC spectrum is consistent with a single direct two-body DPD channel that results in fragments of similar mass and is characterized by a large kinetic energy release (KER) and a broad photoelectron spectrum. The large KER is indicative of substantial repulsion in the radical following photodetachment. The form of the photoelectron spectrum is dominated by the bound to continuum Franck-Condon factors (BCFCF) and is suggestive of photodetachment to a repulsive potential energy surface. A lower bound for the electron affinity of C_2O_4H is reported as 4 eV. BCFCF calculations allow an approximate functional form of the repulsive surface along the $C-C$ stretch coordinate to be extracted from the experimental photoelectron spectrum. PPC spectroscopy of the deuterated analogue ($C_2O_4D^-$), at higher anion beam energies is used to increase the detectability of any possible D atom products, but none are observed.

1 Introduction

The ready decarboxylation of carboxylate radicals is driven by the thermodynamic stability of CO_2 and forms the basis for a number of common synthetic organic transformations, such as the Kolbe electrolysis, the Hunsdiecker reaction and the Barton decarboxylation. [1–3] In the case of a dicarboxylic acid, where intramolecular hydrogen bonding can occur to stabilize both the monoanion and the radical, a question remains as to whether the radical also undergoes ready decarboxylation. Oxalic acid is the simplest possible dicarboxylic acid ($C_2O_4H_2$), and the open shell radical C_2O_4H can be prepared via photodetachment of the precursor $C_2O_4H^-$ monoanion. The stabilizing intramolecular hydrogen bond in the oxalate monoanion has been the focus of a number of theoretical studies [4–7] but no previous work has focused on the effect of H bonding in the radical. In this work it will be shown that C_2O_4H

readily decarboxylates via cleavage of the $C-C$ bond following photodetachment of the monoanion, indicating that the potential for an intramolecular H bond in the neutral is insufficient to stabilize the radical.

If anion photodetachment results in the formation of a neutral on a repulsive potential energy surface it will lead to dissociative photodetachment (DPD). Photoelectron-photofragment coincidence (PPC) spectroscopy couples anion photoelectron spectroscopy with translational spectroscopy of the resulting neutral fragments to produce a kinematically complete picture of DPD. [8] In this manuscript the high beam energy PPC spectrometer; [9] combining an electrospray ionization (ESI) source, a hexapole accumulation ion trap and a linear accelerator (LINAC), is used to study the DPD of the $C_2O_4H^-$ anion. PPC spectroscopy and cold ion photofragmentation spectroscopy have been used to study the DPD of various carboxylate anions including benzoate, naphthoate and acetate, all of which decarboxylate readily following formation of the radical. [10,11] However this is the first study of DPD in a dicarboxylate anion.

Proton transfer is one of the most fundamental of chemical re-

[a] Department of Chemistry and Biochemistry, University of California, San Diego, 9500 Gilman Dr, La Jolla, Ca, 92093-0340. E-mail: rcontinetti@ucsd.edu

actions, with significance in many biological processes.[12,13] Tunneling contributes significantly to the kinetics of proton transfer due to the light mass of the H atom. This is particularly pronounced in the case of a symmetric intramolecular proton transfer such as for the oxalate monoanion, where the product and reactant states are indistinguishable.[5–7] If the intramolecular proton transfer is rapid and the anion is at the transition state between the two indistinguishable conformers of $C_2O_4H^-$, with the H atom equally shared between carboxylate groups for a significant proportion of time, then the three-body DPD products of $H + CO_2 + CO_2 + e^-$ may be favored following photodetachment. However, in the case of a slow proton transfer, where the H is localized on a specific O atom, then two-body DPD products of $HOCO + CO_2 + e^-$ may be expected to dominate in the current PPC spectroscopy study.

There have been multiple theoretical studies probing the dynamics of proton transfer in the oxalate monoanion[4–7] but no direct experimental measurement. Bertrán and coworkers demonstrated that quantum mechanical tunneling contributed significantly to the proton transfer rate, enhanced by the light H atom exchanging between two heavy atoms.[4] Proton transfer occurred more rapidly in malonaldehyde than oxalate due to the hydrogen bond forming a six-membered rather than a strained five-membered ring. Lluch and coworkers determined that the tunneling pathway required concerted heavy atom motion, in this case the motion of the O atom as well as proton motion.[5] Ríos and coworkers used direct ab initio calculations to show that vibrational excitation in the anion could couple to the reaction coordinate and enhance the rate of proton transfer.[6] McCammon and coworkers calculated the barrier height to intramolecular proton transfer as 0.017 eV for hydrogen, 0.05 eV for deuterium and 0.07 eV for tritium. This leads to a lower quantum mechanical tunneling rate for H atoms than the heavier isotopes, as a significant proportion of the hydrogen atoms have sufficient zero-point energy to traverse the barrier classically.[7]

Photoelectron spectroscopy has been used to probe the structure, energetics and dynamics of the gas phase dicarboxylic acid dianions and monoanions, but there have been no previous photoelectron spectroscopy studies of $C_2O_4H^-$. Gutowski and coworkers used negative anion photoelectron spectroscopy and CCSD calculations to study oxalic acid ($C_2O_4H_2$) and reported an adiabatic electron affinity (EA) of 0.72 eV and a vertical detachment energy of 1.08 eV.[14] The neutral and anion ground states were calculated to have similar geometries, with a planar C_{2h} structure where both H atoms are oriented between the two carboxyl groups, stabilized by two intramolecular H bonds. The authors concluded that the valence anion state was stabilized by the nature of the singly occupied molecular orbital that exhibits a bonding $C-C$ interaction and an antibonding $C-O$ interaction. The proximity of the carboxylic acid groups facilitated the bonding interaction resulting in the large electrophilicity of the oxalic acid. Additionally, H bonds and buckling of the molecular framework can stabilize the valence anionic states.[14]

Low-temperature ESI photoelectron spectroscopy has been used by Wang and coworkers to probe the structure of the longer aliphatic dicarboxylic monoanions ($HO_2C(CH_2)_nCO_2^-$ where $n =$

$1 - 10$).[15] Similar features were seen in all the photoelectron spectra, where bands corresponded to detachment from the oxygen lone pairs and yielded adiabatic detachment energies (ADE) around 4.5 eV, indicating that the aliphatic chain length had little influence on the binding energy of the carboxylate group. The ADE is ≈ 1 eV higher than for the monocarboxylate analogues,[16] indicating that the dicarboxylate anions were more stable due to the intramolecular H bond between the terminal carboxylic acid and carboxylate groups. A long tail was observed to the low binding energy side of the spectra indicating a large geometry change between the anion and the neutral. This was attributed to the weaker hydrogen bonding in the neutral than the anion due to the lower electron density localized on the oxygen atom. The measurements were repeated at 70 K and 350 K, with no significant difference observed at the two temperatures. No vibrational structure was resolved, but a small blue shift was noted as the H bond was stabilized by an entropic effect at the higher temperature. The ADE varied slightly with chain length, reaching a minimum for the most strained conformer ($n=5$), as the backbone has to contort the most to accommodate the hydrogen bond. Calculations showed that cyclic conformers are preferred over linear as they facilitate hydrogen bonding.[15]

Wang and coworkers have also used photoelectron spectroscopy to probe the water clusters of the oxalate dianion $C_2O_4^{2-}(H_2O)_n$, where $n = 4 - 40$.[17,18] The dianion was shown to be at the center of the water cluster, and as water molecules were added to the solvation shells, the intensity of photoemission from the dianion was reduced. The measured electron binding energies increased with cluster size and the high binding energy cutoff for electron emission was determined by the repulsive Coulomb barrier (RCB) that exists universally in multiply charged anions, and prevents slow electrons from being emitted.[19,20] In the larger clusters a high binding energy feature was seen to grow in, attributed to ionization of the water solvent as the ionization potential of water was lowered significantly by the negatively charged clusters.[17] This study was expanded upon in a later report by the same group.[18] The mass spectrum indicated that three water molecules are required to stabilize the $C_2O_4^{2-}$ moiety, where the $n = 3$ cluster has an ADE of 0.0 eV. Calculations showed that the first four water molecules bind tightly to the oxalate dianion with a pair of hydrogen bonds each, the fifth and sixth water molecules bind by a single hydrogen bond to the dianion, before water-water hydrogen bonding dominates. Photon energy dependent measurements allowed the RCB height to be determined and it was reported to decrease with increasing physical size of the cluster, as the two equal charges are more effectively stabilized. The bare dianion had a twisted structure (D_{2d}) and a torsion angle that decreased upon solvation.[18]

There has been no direct measurement of the EA of the C_2O_4H neutral. Vairamani and coworkers estimated the gas phase acidity (AH $\longrightarrow H^+ + A^-$) of a series of dicarboxylic acids, including oxalic acid, using the kinetic method.[21] The gas phase acidity of $C_2O_4H_2$ was determined to be larger than expected (13.71 eV), due to stabilization of the anion by a weak intramolecular hydrogen-bond and the formation of a five-membered ring. The gas phase acidity can be used to extract an EA of 4.44 ± 0.12 eV

	Relative Energy, eV	C−C bond length, Å	Energy, E_h	Zero point energy, E_h
$C_2O_4H^-$ $^1A'$	0	1.58	-376.9615	0.0368
$C_2O_4H^-$ ^1A	0.37	1.55	-376.9471	0.0359
$C_2O_4H^-$ $^1A'$	0.49	1.59	-376.9428	0.0360
C_2O_4H $^2A'$	4.36	1.54	-376.7996	0.0353
$t-HOCO + CO_2 + e^-$	3.15	-	-376.8401	0.0311
$c-HOCO + CO_2 + e^-$	3.22	-	-376.8373	0.0308

Table 1 The calculated energies, zero point energies and where applicable the C−C bond lengths of the anion, neutral and dissociation asymptotes. The symmetry of each electronic state (singlet for the anion and doublet for the neutral) is shown.
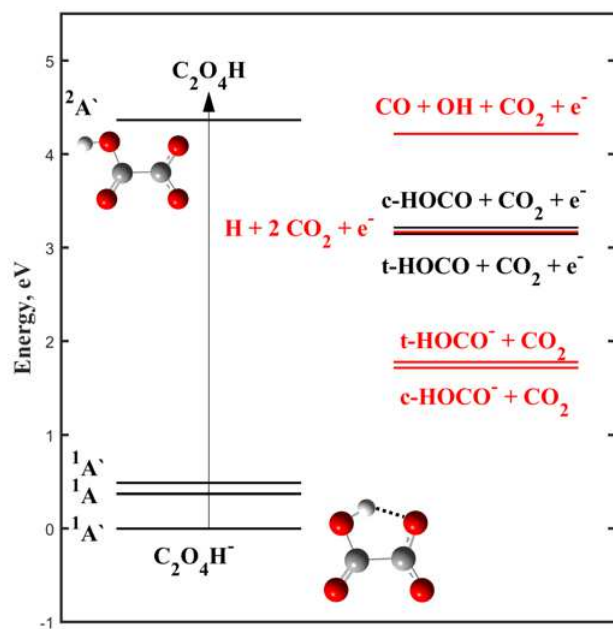
Fig. 1 The calculated relative energies of the anion states, neutral states and dissociation asymptotes in black. The other asymptotes in red are calculated from the known energetics of HOCO and HOCO$^-$, and plotted relative to the calculated $t-HOCO + CO_2 + e^-$ asymptote.[23,24] The calculated structures of the anion and neutral ground state are also shown.

for the C_2O_4H neutral.[22] In this manuscript the results of the high beam energy PPC spectroscopy study on the oxalate monoanion will be reported. This is the first photoelectron spectroscopy study of the smallest dicarboxylic acid monoanion. The dissociation dynamics at 4.66 eV will be shown to be dominated by a single two-body DPD channel resulting in $HOCO + CO_2 + e^-$.

2 Structure and energetics of $C_2O_4H^-$ and C_2O_4H

The structure of the $C_2O_4H^-$ and $C_2O_4^{2-}$ anions, in the gas and crystalline phases, has been calculated by Dewar and Zheng using AM1 and ab initio models.[25] Two isomers of $C_2O_4H^-$ were reported with similar energies. The first is a planar structure with a 0° twist angle between the CO_2 groups and the O−H bond oriented towards the carboxylate group, and the second form is orthogonal, with a 90° twist angle between CO_2 groups and the O−H bond oriented away from the rest of the molecule. Only the first planar isomer is able to be stabilized by an intramolecular hydrogen bond, and undergo intramolecular proton transfer.

More recently Kabeláč and coworkers used ab initio quantum calculations in the gas phase to find two minima in the $C_2O_4H^-$ potential energy surface.[26] The global minimum is planar with the H bond oriented towards the carboxylate group and the first excited state is twisted with the O−H bond oriented away from the molecular framework. The ground state is stabilized by a weak intramolecular hydrogen bond and the first excited state is 0.43 eV above the ground state. The structures are similar to those reported by Dewar and Zheng, but the relative energies are significantly different. Rotation about the C−C bond is calculated to be hindered by the hydrogen bond (barrier 0.26 eV) and the rotation of the O−H group is blocked (barrier 0.93 eV).

Figure 1 shows the energy levels of the $C_2O_4H^-$ anion, the C_2O_4H neutral, the dissociation asymptotes of the photodissociation and DPD product channels and the photon energy. The energy levels shown in black are the result of geometry optimization and energy calculations, zero-point energy corrected, using the coupled cluster CCSD(T) method and an aug-cc-pVDZ basis set. All the calculations were carried out using the Gaussian 16 suite of programs.[27] Energy levels shown in red are calculated from literature values of the EA and bond dissociation energy of HOCO relative to the calculated $t-HOCO + CO_2 + e^-$ asymptote, where $c/t-HOCO$ are the cis- and trans- isomers of HOCO.[23,24]
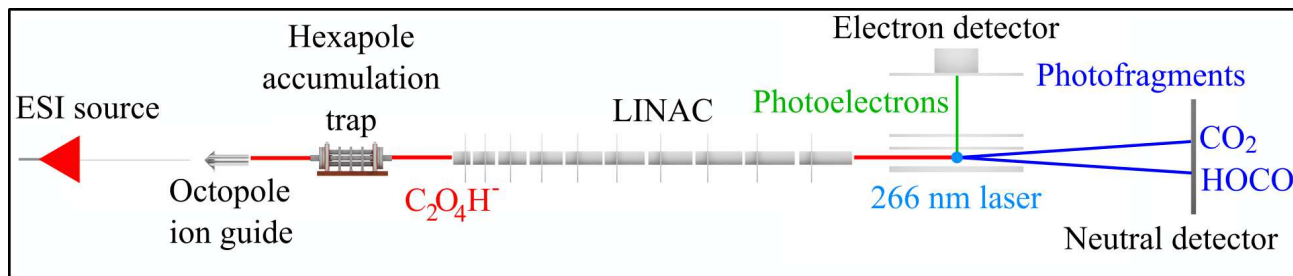
Fig. 2 Schematic of the principal elements of the high beam energy PPC spectrometer.

There are three anion minima, and the neutral ground state is accessible with a single 266 nm (4.66 eV) photon from any of them.

The calculated anion global minimum structure, shown in Fig. 1, is similar to the energy minimum predicted by both Zheng and Kabeláč. The O−H bond is oriented towards the carboxylate group to form an intramolecular hydrogen bond which stabilizes the anion at the expense of accommodating a strained five-membered ring. All of the anion minima are singlets. Two other local minima were found, the first with a planar structure and the second with a twisted geometry, both of which have the O−H bond oriented away from the carboxylate group. The second excited state is similar to the local minima reported by Zheng and Kabeláč, with a relative energy of 0.49 eV (Kabeláč reported 0.43 eV). The first excited minimum has not been reported before.

The open shell C_2O_4H neutral has a minimum with a shorter C−C bond length than the anion minimum, and the O−H group oriented away from the other carboxylate group. The neutral minimum was located via geometry optimization and energy minimization calculations initialized at the geometry of the first excited anion state, after the removal of an electron. The minimum energy structure for the doublet neutral is not stabilized by an intramolecular hydrogen bond. In this case the $O \cdots H-O$ interaction would be weaker than the $O^- \cdots H-O$ in the anion analogue, due to the lower electron density on the O atom. This weaker H bond does not stabilize the neutral sufficiently to compensate for the strain induced by the formation of a five-membered ring, especially as the strain would be larger than in the anion form due to the shorter C−C bond length. In order to mimic the vertical transition observed upon photodetachment of the anion, energy minimization calculations were performed starting from the anion minimum energy structure after the removal of an electron. These calculations resulted exclusively in t-HOCO + CO_2, indicating that the hydrogen-bonded five-membered ring neutral structure is high in energy and repulsive in character. The neutral minimum is energetically above all of the probable dissociation asymptotes resulting from C−C bond cleavage, but the calculations indicate that it is bound, suggesting a high energy transition state on the neutral surface. One possible explanation is that the transition state for dissociation of the neutral minimum is similar to the high-energy, dissociative neutral structure accessed via a vertical transition from the anion ground state, where the repulsive potential energy surface intersects the bound surface at high energy. In this case the dissociation of the neutral minimum would proceed via rotation of the OH group where a significant

barrier is observed for a similar rotation on the anion potential energy surface. This is similar to the potential energy surfaces of the formyloxyl radical where evidence is seen for a long lived HCO_2 neutral in the photoelectron spectrum, despite the radical being higher in energy than the observed dissociation asymptotes of H + CO_2.[28,29] In that case the HCO_2 neutral is bound with respect to OH + CO, but predissociation to produce H + CO_2 occurs in vibrationally excited HCO_2 where repulsive potential energy surfaces intersect with the bound energetic minimum. Calculations were attempted to find the geometry and energy of the first excited neutral state, but convergence was not achieved, due to the difficulty in performing open shell electronic structure calculations. There have been no previously reported calculations on the neutral C_2O_4H potential energy surface. Single point energy calculations at the optimized anion and neutral geometry indicate an EA of 4.36 eV.

Multiple dissociation channels are energetically accessible at a photon energy of 4.66 eV including the CO_2 + $HOCO^-$ photodissociation channel, the CO_2 + HOCO + e^- two-body DPD channel and the two three-body DPD channels yielding CO_2 + CO_2 + H + e^- and CO_2 + CO + OH + e^-. The HOCO anion and radical have been studied extensively using PPC spectroscopy.[23,24,30] From the D_0 of c−HOCO (0.99 ± 0.02 eV) and t−HOCO (1.07 ± 0.02 eV) the difference between the neutral isomers is 0.08 ± 0.04 eV.[23] The EA of c−HOCO is 1.51 ± 0.01 eV, and t−HOCO is 1.37 ± 0.01 eV. Therefore, the c−$HOCO^-$ anion is more stable than the trans, but the t−HOCO neutral is more stable than c−HOCO. The calculations presented here predict a relative energy of the c− and t−HOCO isomers of 0.07 eV, within the error of the experimental value. The c−HOCO radical lies above the H + CO_2 dissociation asymptote but is long-lived due to a large barrier to dissociation, which can be slowly tunneled through.[30] There is no direct low-energy path from t−HOCO to the H + CO_2 dissociation products, so typically isomerization to either c−HOCO or the HCO_2 radical occurs,[28,29] the latter of which readily dissociates. The barrier to isomerization between the isomers of HOCO is predicted to be 0.36 eV above the t−HOCO. Both isomers of HOCO are more than 1 eV lower in energy than the CO + OH product asymptote.[30]

Table 1 shows energies, zero point energies and, where applicable, the C−C bond lengths of the anion, neutral and dissociation asymptotes. The large change in C−C bond length between the anion ground state (1.58 Å) and the neutral ground state (1.54 Å) and the reorientation of the O−H bond is likely to yield poor Franck-Condon overlap at the anion equilibrium geometry. The

other anion local minima also have longer C−C bond lengths than the neutral global minimum. As all of the energetically accessible dissociation pathways result in C−C bond breaking, photodetachment of the anion is likely to yield a neutral with an elongated C−C bond progressing along the dissociation coordinate.

3 Experimental methods

The high beam energy PPC spectrometer, shown in Fig. 2, has been described in detail elsewhere.[9] Briefly the oxalate monoanions are produced via ESI of a solution of 2 mmol $C_2O_4H_2 \cdot (H_2O)_2$ ($C_2O_4D_2$ for the $C_2O_4D^-$) in methanol, and desolvated in a heated capillary. The anions are accumulated in a hexapole RF trap, thermalized with room-temperature He buffer gas, and extracted at a 50 Hz repetition rate. Anions are funneled into the LINAC and accelerated using 10 sequential acceleration stages to either 11 keV, 16 keV or 21 keV.[31] Increasing the beam energy increases the detection efficiency of any light neutral fragments, and improves the discrimination against false coincidences.[32] The anions are photodetached with the fourth harmonic of a mode-locked, Q-switched, cavity dumped Nd:YAG laser (266 nm) or the third harmonic of a Ti:Sa regenerative amplifier (258 nm).[33] The x, y arrival positions of the photoelectrons are recorded as a photoelectron image capturing the angular distributions. The electron arrival time is also recorded.[34] From this information the electron kinetic energy (eKE) spectra can be extracted. The arrival position and time of up to three neutral fragments are recorded on the neutral detector. The kinetic energy release (KER) spectrum can be extracted from this data for any pairs or triples of fragments originating from the same dissociating anion. As the photoelectrons are recorded in coincidence with the neutral fragments from the same anion a 2D histogram of N(eKE, KER) can be plotted, known as a PPC spectrum.[8] The undetached anions are deflected out of the neutral beam and onto an ion detector to be monitored in real time.

4 Results

PPC spectroscopy measurements on $C_2O_4H^-$ are reported at multiple beam energies (11 keV, 16 keV and 21 keV) and wavelengths (266 nm and 258 nm). Photoelectron images, eKE spectra, KER spectra and PPC spectra were recorded. Additionally total energy spectra ($E_{TOT} = eKE + KER$) can be extracted from the data. Initially the results for 11 keV $C_2O_4H^-$ photodetached at 266 nm will be reported in detail. A brief overview of the results for the studies utilizing a higher photon energy, higher anion beam energies and the deuterated analogue ($C_2O_4D^-$) follow.

4.1 PPC spectroscopy of 11 keV $C_2O_4H^-$ at 266 nm

Figure 3 shows the total photoelectron spectrum for 11 keV $C_2O_4H^-$ recorded at 266 nm in blue. It peaks at eKE= 0 eV and extends as a single feature to eKE= 0.8 eV. The broad form of this spectrum indicates a significant change in geometry from the anion to the neutral, and a lineshape dominated by the bound-continuum Franck-Condon factors that govern photodetachment. It is difficult to extract an exact EA from this photoelectron spectrum due to the lineshape, but higher eKE electrons are recorded

than would be expected from the calculated EA. It is possible to extract a lower limit of the EA from the photoelectron spectrum, EA(C_2O_4H) ≥ 4 eV, whilst accounting for the likelihood of hot-bands in the spectrum. As PPC spectroscopy is a coincidence technique it is possible to distinguish photoelectrons detached from neutrals that subsequently dissociate, from those that remain stable. In red in Fig. 3 is the dissociative photoelectron spectrum containing the photoelectrons that arrive in coincidence with two or more neutral fragments. It is identical to the total photoelectron spectrum, indicating that the neutral always dissociates following photodetachment. The broad spectrum observed is consistent with photodetachment onto a repulsive potential energy surface.

There are two clear wings in the neutral fragment time of flight spectrum (ESI† Fig. S1) for 11 keV $C_2O_4H^-$ at 266 nm. The spectrum peaks at $t = \pm 80$ns with little intensity at $t = 0$s. The wings indicate that dissociation is occurring, with neutral fragments recoiling forwards and backwards along the ion beam propagation and laser electric vector direction. Any stable C_2O_4H produced following photodetachment would arrive at $t = 0$. By considering the arrival times and positions of the pairs of neutral fragments it is possible to calculate a fragment mass spectrum. Fig. 4a shows the fragment mass spectrum of 11 keV $C_2O_4H^-$ recorded at 266 nm and indicates two fragments of similar masses, centered at 44 a.m.u. The mass of CO_2 and HOCO are 44 and 45 a.m.u. respectively, both within the 10% mass resolution of the neutral detector, consistent with the production of $HOCO + CO_2 + e^-$.

Events are classified by the number of neutral fragments that arrive in coincidence with a photoelectron. In this case only two-body processes are observed, with no evidence seen for three-body dissociation. Following dissociation the pairs of fragments recoil from the center-of-mass velocity leading to the wings in the time of flight spectrum and a distribution of neutral fragment arrival positions across the neutral detector, as shown in Fig. 2. Fig. 4b shows the two-body KER spectrum for the dissociation of 11 keV $C_2O_4H^-$ following irradiation at 266 nm in blue. It is a featureless peak, with maximum intensity at 1.1 eV. The large KER indicates significant repulsion in the transition state driving dissociation, as photodetachment results in a neutral on a steeply repulsive portion of the potential energy surface. The lack of vibrational structure in the KER spectrum is also consistent with dissociation occurring on a purely repulsive surface, rather than via a metastable neutral state.

The high beam energy PPC spectrometer allows the acceleration potential applied to the parent anions to be readily altered. Increasing the beam energy increases the detection efficiency of light neutral fragments resulting from DPD. In this case increasing the beam energy should make any hydrogen atoms produced via a three-body DPD process more detectable, however only two-body DPD was seen at all beam energies, with no evidence observed for H atom production. Fig. 4b shows the KER spectra for 11 keV, 16 keV and 21 keV $C_2O_4H^-$ at 266 nm. The three spectra are very similar indicating that dissociation is prompt on the time scale of the flight time between the interaction region and the neutral detector ($\approx 10\,\mu$s). A small shift in the peak KER (≤ 0.05 eV) is seen at 21 keV, attributed to a small change in detector acceptance
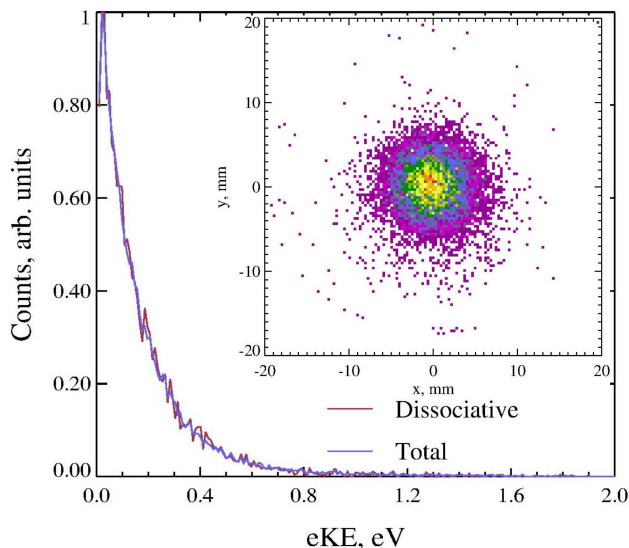
Fig. 3 The total (red) and dissociative (blue) photoelectron spectra for 11 keV $C_2O_4H^-$ at 266 nm. The inset is the total photoelectron image.

Fig. 4 a) The mass spectrum for two neutral fragments produced during photodetachment of 11 keV $C_2O_4H^-$ at 266 nm. b) The KER spectrum of $C_2O_4H^-$ recorded at 266 nm and multiple beam energies.

function at the higher beam energy.

Figure 5 is the PPC spectrum for 11 keV $C_2O_4H^-$ at 266 nm. There is a single broad Gaussian-like feature centered at (KER, eKE) $=(1.1$ eV, 0.2 eV), consistent with a single dissociation channel. The diagonal form of the high total energy feature is consistent with a constant total energy available to partition between the kinetic energy of the photoelectrons and neutral fragments. The presence of vibrational excitation in the parent anions broadens the distribution to higher energies, whereas internal excitation in the products broaden the distribution to lower energies. The black lines are the calculated maximum kinetic energy (KE_{max}) available to partition between the photoelectron and the neutral fragments if DPD results in t$-$HOCO$+CO_2+e^-$ (solid line) and c$-$HOCO$+CO_2+e^-$ (dashed line). The KE_{max} for DPD resulting in the CO_2+t$-$HOCO$+e^-$ products is calculated using,

$$KE_{max} = h\nu - E_{\text{t-HOCO}+CO_2}$$
$$= 1.51 \text{ eV} \tag{1}$$

where $h\nu$ is the photon energy and $E_{t-HOCO+CO_2}$ is the energy of the dissociation asymptote relative to the calculated anion ground state. Analogously, for the c$-$HOCO$+CO_2+e^-$ dissociation asymptote, $KE_{max} = 1.44$ eV. Both KE_{max} match well with the high total energy side of the intense feature in the PPC spectrum providing strong evidence for two-body DPD resulting in HOCO$+CO_2$. However as the two isomers of HOCO are similar in energy it is not possible to determine which is being preferentially formed from the KE_{max} alone, due to the 12% energy resolution of the spectrum.

Additionally the DPD feature in the PPC spectrum (Fig 5) extends beyond the KE_{max} indicating some vibrational excitation in the anions. This is clarified by the inset of Fig. 5 which plots the E_{TOT} spectrum of 11 keV $C_2O_4H^-$ at 266 nm. Again the black lines show the calculated KE_{max} for the different isomers of HOCO, and the high energy tail indicates hot anions. Previous studies have
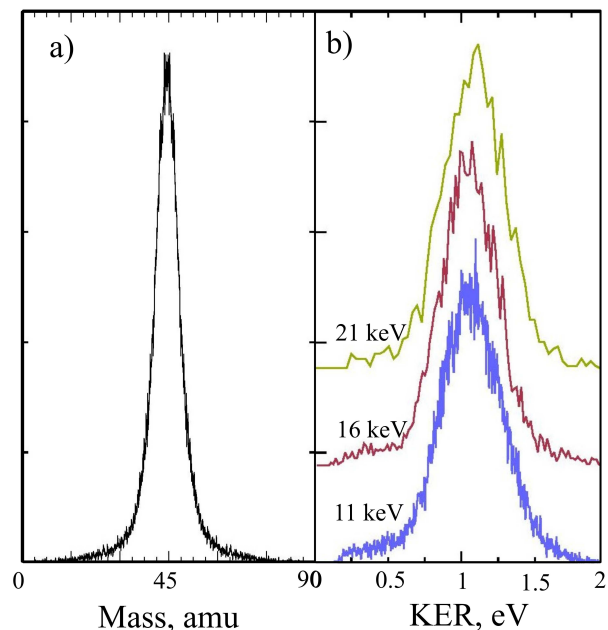
indicated that the anions in this apparatus are characterized by a vibrational temperature of 298K as the anions are thermalized with the room temperature buffer gas in the hexapole accumulation trap.[9] The presence of substantial intensity below the KE_{max} is consistent with vibrational excitation in the neutral products. The shift in the peak value of the E_{TOT} distribution from the calculated KE_{max} is ≈ 0.3 eV, sufficient energy to excite a C$-$O stretch or bending mode in either CO_2 or HOCO.[23,35] From the PPC spectrum it is not possible to determine if a particular vibration is preferentially excited, which may be a result of the energy resolution of the spectrum or simultaneous excitation of multiple vibrational modes in the parent anions and the products.

4.2 PPC spectroscopy of $C_2O_4H^-$ at 258 nm, and $C_2O_4D^-$

The PPC spectrum for 11 keV $C_2O_4H^-$ at 258 nm (ESI† Fig. S2) is very similar to the PPC spectrum recorded at 266 nm shown in Fig. 5. The higher photon energy increases the amount of energy available to partition between the photoelectrons and the neutral fragments, and shifts the single broad feature to higher eKE. However no additional features grow in, indicating DPD resulting in HOCO$+CO_2+e^-$ still dominates the dynamics and occurs via the same electronic state. The same single feature is seen in the PPC spectra for 16 keV and 21 keV $C_2O_4H^-$ (ESI† Fig. S3) as in Fig. 5 indicating two-body DPD to HOCO$+CO_2+e^-$, as expected from the similar KER spectra shown in Fig. 4b.

Increasing the beam energy of the parent anion increases the detectability of fragments, but very light fragments such as hydrogen atom fragments are still challenging to detect. As one possible energetically accessible three-body DPD channel is $CO_2+CO_2+H+e^-$, it was necessary to increase the detectability of the H atoms as far as possible. Analogous experiments
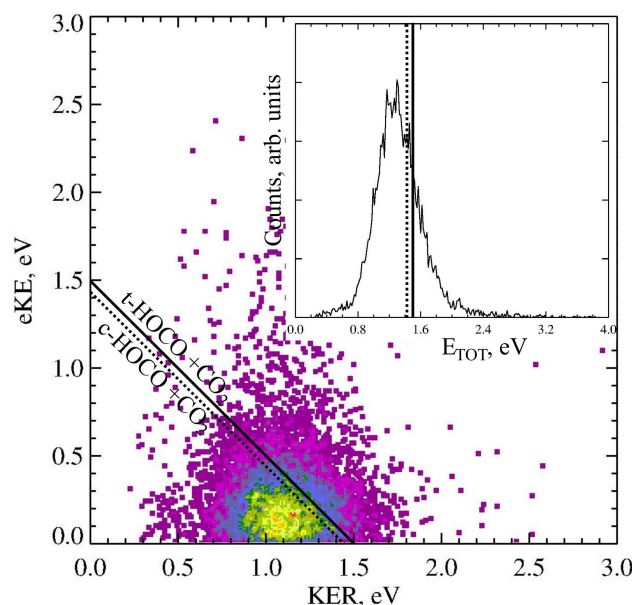
Fig. 5 The PPC spectrum for 11 keV $C_2O_4H^-$ at 266 nm. The inset is the E_{TOT} spectrum. The diagonal lines show the KE_{max} for both isomers of HOCO.

were carried out on deuterated analogue ($C_2O_4D^-$) to increase the mass and therefore detectability of any D atom products. No evidence was seen for a three-body channel. The two-body PPC spectrum for 21 eV $C_2O_4D^-$ 266 nm (ESI†, Fig. S4) contains only the same feature as the 11 keV $C_2O_4H^-$ PPC spectrum shown in Fig. 5, consistent with a single two-body DPD channel producing $DOCO + CO_2 + e^-$.

5 Discussion

The PPC spectroscopy measurements presented here indicate a single dissociation channel is operative at a photon energy of 4.66 eV, resulting in two fragments of roughly equal mass, assigned to direct two-body DPD producing $HOCO + CO_2 + e^-$. In this section the results will be discussed to extract information about the EA of C_2O_4H, the assignment of the dissociation channel and the preferred isomer of HOCO, before bound-continuum Franck-Condon factor calculations are presented to determine an approximate form of the repulsive electronic state.

5.1 Photoelectron Spectroscopy

The identical feature at low eKE in the total and dissociative photoelectron spectra in Fig. 3 indicate that no stable C_2O_4H is formed. This is confirmed by analysis of the time of flight spectrum, and the raw neutral detector image. The calculations presented in section 2 indicate that the neutral ground state ($^2A'$) should be energetically accessible from the anion ground state ($^1A'$), with an EA of 4.36 eV. However, the neutral is calculated to have a shorter C−C bond length than the anion, and so it may be the case that the vertical detachment energy to the ($^2A'$) state from the anion equilibrium geometry is larger than the photon energy. If the bound state is energetically accessible with a 4.66 eV photon it may be the case that the Franck-Condon overlap to the

bound neutral is negligible from the equilibrium geometry of the anion particularly as the reorientation of the O−H bond is required, with the breaking of a H bond. It is clear from this that the potential for intramolecular hydrogen bonding is not sufficient to stabilize the radical and prevent facile decarboxylation driven by the thermodynamic stability of the CO_2 molecule. Nonetheless the calculations indicate that a bound form of C_2O_4H exists, but it is not accessible via a vertical transition from the anion's equilibrium geometry at this photon energy. Additionally, any vibrational excitation of the room temperature anions is likely to increase the C−C bond length further still, increasing the preference for dissociation.

As described in the introduction, Wang and coworkers have recorded the photoelectron spectrum for a series of aliphatic dicarboxylic acid monoanions, the shortest being $HO_2CCH_2CO_2^-$.[15] In that study photodetachment was found to occur primarily from the CO_2^- group, as would also be expected for $C_2O_4H^-$. The ADE for the longer dicarboxylate monoanions was found to range from $4.41 - 4.69 \pm 0.05$ eV, higher than seen for the $C_2O_4H^-$ observed in this study. The low intensity tail extends to 0.8 eV indicating that the E.A. of C_2O_4H is nearer 4 eV. This indicates a weaker intramolecular H bond in the oxalate anion than the longer chain analogues, where the sp^2 hybridized terminal carbons are linked via at least one sp^3 hybridized carbon. In the case of the longer chain systems the carbon backbone can distort to accommodate the optimal geometry of the H bond, whereas in the $C_2O_4H^-$ case the anion geometry is determined by the planar orientation of the sp^2 hybridized C−C bond, resulting in a longer H bond. The five-membered ring formed via the hydrogen bond in C_2O_4H is strained, reducing the stability of the ion. It is clear though that the intramolecular H bond between the two carboxylic acid groups does still stabilize the oxalate anion, as the ADE is significantly higher than for the aliphatic carboxylate anions of the form $CH_3(CH)_nCO_2^-$, where only a very weak C−H···O intramolecular hydrogen bond is possible.[36]

5.2 Two-body vs three-body DPD

At 266 nm there are a number of energetically accessible dissociation pathways resulting in neutral fragments and electrons as shown in Fig. 1. There is an observed two-body channel resulting in roughly equal mass fragments of $HOCO + CO_2 + e^-$, which can occur either via direct DPD or via a sequential two-photon process of photodissociation and subsequent photodetachment. The KE_{max} on the PPC spectrum in Fig. 5 are the calculated values for direct DPD from the anion ground state to the different isomers of HOCO. In the case of sequential two-photon photodissociation and photodetachment the total energy available to partition between the electron and the fragments would be far larger i.e. $KE_{max} = 2h\nu - 3.15$ eV $= 6.17$ eV. The most intense portion of the PPC spectrum would be approximately located at (eKE, KER)$< (3.2$ eV$, 2.9$ eV$)$, assuming that all the excess energy from the first photon following photodissociation of the C−C bond is transferred to the KER, and all excess energy from the second photon following photodetachment of the $HOCO^-$ is transferred to the eKE. This is unlike the experimentally observed PPC spec-

trum, and provides strong evidence for direct DPD rather than two-photon photodissociation and photodetachment. It is possible that $C_2O_4H^-$ undergoes two-body photodissociation, as has been observed in other carboxylic acids.[11] However at the low laser power used in this study the one-photon products of a single neutral and anionic fragment would be favored, where only the neutral fragment is detectable in a PPC experiment. In this case the presence of such a channel cannot be conclusively determined.

There are two energetically accessible three-body DPD channels resulting in $CO_2 + CO + OH + e^-$ and $CO_2 + CO_2 + H + e^-$. No data was observed indicating three neutral fragments in coincidence with an electron, originating from a single anion, suggesting that neither of these channels are accessed. For the former channel where all the fragments have $m > 17$ a.m.u., this is conclusive evidence against its occurrence. Great effort was expended, as detailed in the results section, to increase the detectability of the light neutral H atoms, by increasing the beam energy of the $C_2O_4H^-$ anions and using a deuterated analogue, but no H or D atoms were detected. It is plausible that the three-body channel was occurring but the light H atom fragment was recoiling outside the active area of the detector, and therefore the two $CO_2 + CO_2$ fragments that were detected would be indistinguishable from the $HOCO + CO_2$ fragments due to the mass resolution of the neutral detector. However, in that case the momentum partitioning to the H atom would be significant, such that a large proportion of the KER would be undetected. In this case a significant discrepancy between the theoretical $KE_{max}(CO_2 + CO_2 + H) = 1.46$ eV, using $E(c-HOCO^- \rightarrow CO_2 + H + e^-) = 1.49$ eV[24] and $D_0(C_2O_4H^- \longrightarrow c-HOCO^- + CO_2) = 1.71$ eV, and the observed two-body KE_{max} in the PPC spectrum would be expected, which is not observed. From the exclusive observation of two-body DPD channels it may be inferred that the rate of proton transfer in the oxalate monoanion is relatively slow and that the proton is localized on one of the carboxylate groups. It may be the case that at higher excitation energies other repulsive electronic states are accessible which would lead directly to three-body dissociation. Additionally, selectively vibrationally exciting the $O-H$ stretch of the $C_2O_4H^-$ anion via IR excitation may induce a preference for three-body dissociation.

5.3 Prevalent HOCO isomer

From Fig. 5 it is clear that DPD results in $HOCO + CO_2 + e^-$ but the prevalent HOCO isomer cannot be determined given the energy resolution in the experiment. Additionally vibrational excitation of the room temperature anions gives significant width to the E_{TOT} spectrum, as there are a significant number of low frequency vibrational modes populated at 298 K, making it difficult to determine whether a single HOCO isomer is preferentially formed or a mixture.

Despite the experiment being unable to distinguish between the isomers, it would be expected that simple $C-C$ bond cleavage of the $C_2O_4H^-$ ($^1A'$) structure would preferentially result in the $t-HOCO$ isomer, due to the large barrier to rotation of the OH group. After the removal of an electron from the mini-
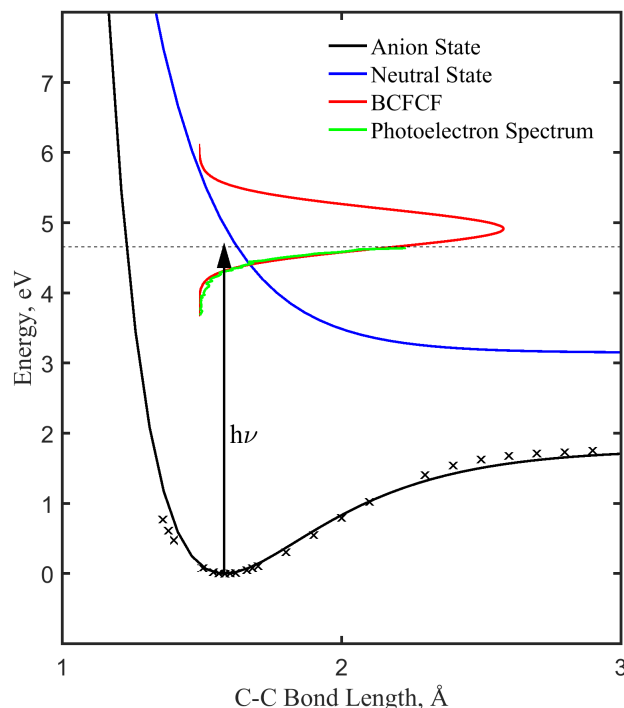
Fig. 6 The calculated anion ground state in black crosses, with the Morse potential fit shown as a black curve, the neutral repulsive surface in blue, the calculated BCFCF in yellow and the dissociative photoelectron spectrum in green.

mum energy geometry of $C_2O_4H^-$ ($^1A'$), geometry optimization calculations using the methodology described in section 2 resulted in $CO_2 + t-HOCO$. Additional evidence for a preference for $t-HOCO$ is found in the observation of no three-body dissociation to $H + CO_2 + CO_2$, either directly via concerted $C-C$ and $O-H$ bond breaking, or by subsequent dissociation of the HOCO radical. As seen in the energetics in Fig. 1 the asymptote for dissociation to $c-HOCO + CO_2$ lies above the asymptote for $H + CO_2 + CO_2$ where dissociation occurs via tunneling through the barrier. The barrier between $t-HOCO$ and $CO_2 + H$ is substantially higher than for $c-HOCO$ and so isomerization to $c-HOCO$ or HCO_2 is the predominant route for dissociation of $t-HOCO$.[30] Therefore, it is more likely that $t-HOCO$ will remain stable on the timescale of the flight time from the interaction region to the detector, as it would have to isomerize prior to dissociation.

5.4 Repulsive electronic states of C_2O_4H

No previous studies have calculated the form of the repulsive potential energy surface that leads to the rapid dissociation of the C_2O_4H neutral to $CO_2 + HOCO$. It is clear from the data presented here that the state is very repulsive in the Franck-Condon region, due to the large KER. The distribution of events along the diagonal cutoff in the PPC spectrum at high E_{TOT} indicates that a relatively narrow range of anion geometries lead to dissociation. Additionally, the dissociative photoelectron spectrum is dominated by a single broad, structure-less feature, with a line shape dominated by the bound-continuum Franck-Condon factors (BCFCF).

LeRoy's BCONT formalism can be used to calculate the bound-continuum Franck-Condon factors for diatomic molecules.[37,38] As $C_2O_4H^-$ undergoes DPD to form two fragments with similar masses via cleavage of a single bond, it is approximated to a diatomic molecule here. Fig. 6 plots the results of the $C_2O_4H^-$ ground state potential energy calculations varying the $C-C$ bond length and the Morse fit to the anion ground state, the repulsive neutral surface leading to $CO_2 + HOCO$, the BCFCFs calculated using the BCONT program and the experimental photoelectron spectrum. Electronic structure calculations (Gaussian16, CCSD(T)) were used to calculate the form of the anion ground state by scanning the $C-C$ bond length and minimizing the energy whilst constraints on the other degrees-of-freedom were relaxed. This curve was then fit with a Morse potential (ESI† Equation 1, Table S1) for an optimal fit near the anion equilibrium geometry. In this case the harmonic frequency was used as a fitting parameter where the starting point was the calculated $C-C$ stretch in $C_2O_4H^-$ ground state. The repulsive state was constrained to the calculated dissociation asymptote of $t-HOCO + CO_2 + e^-$, and the form of the potential was optimized to match the BCFCF with the experimentally measured dissociative photoelectron spectrum (ESI† Equation 2, Table S2). The steeply repulsive potential energy surface results in BCFCF with intensity over a wider energetic range than the observed photoelectron spectrum, due to the high energy cutoff of the experimental spectrum by the photon energy. Previous photoelectron spectra of the long chain aliphatic dicarboxylic acid monoanions, reported by Wang and coworkers, indicated excited electronic states lying significantly above the photon energy used here. In the future these experiments will be repeated at a higher photon energy to probe the full Franck-Condon envelope, and assess the presence of higher lying excited electronic states.

The observation of $HOCO + CO_2 + e^-$ products with a large KER suggests significant repulsion driving the dissociation, and the BCONT calculations are consistent with a steeply repulsive potential energy surface. However, calculations described in section 2 indicated the presence of a neutral minimum with a shortened $C-C$ bond compared to the anion. If this anion geometry was leading to dissociation it may be expected that the repulsion in the transition state would be reduced by the elongation of the $C-C$ bond, in contrast to the observed large KER. However, a vertical transition from the anion ground state geometry would result in a neutral with a weakly hydrogen-bonded, five-membered ring structure, which is shown to be high in energy and dissociative in character. It may be that the strain induced in the neutral molecular framework by the five-membered ring, in the absence of a strong hydrogen bond, drives the dissociation. No experimental evidence was seen for the production of a stable radical, showing there is no Franck-Condon overlap with the calculated bound state. If the bound neutral requires rotation of the OH group in order to undergo dissociation, it may dissociate via a high energy transition state similar to the neutral state accessed by a vertical transition from the anion ground state geometry. Further theoretical work is required to fully understand the potential energy landscape of this system.

6   Conclusions

The dissociation dynamics of $C_2O_4H^-$ have been studied for the first time using PPC spectroscopy measurements at 266 nm, 258 nm and multiple beam energies. No stable C_2O_4H was produced, and the only product channel observed was direct two-body DPD to $HOCO + CO_2 + e^-$. The potential for the H-bond in the neutral is not sufficient to stabilize the oxalate radical with respect to decarboxylation. BCFCFs were calculated that reproduce the dissociative photoelectron spectrum, and show that the dissociative potential energy surface is steeply repulsive. No three-body DPD producing either $2CO_2 + H + e^-$ or $CO_2 + OH + CO + e^-$ was observed, either at higher beam energies or with the deuterated analogue, both of which would increase the detection efficiency of the H/D atom. In the future this study will be built upon to investigate the DPD of long chain dicarboxylic acids, both monoanions and dianions.

Conflicts of interest

There are no conflicts to declare.

Acknowledgments

Notes and references

1   H. Kolbe, Justus Liebigs Annalen der Chemie, 1849, **69**, 257–294.

2   D. H. R. Barton, H. A. Dowlatshahi, W. B. Motherwell and D. Villemin, J. Chem. Soc., Chem. Commun., 1980, 732–733.

3   R. G. Johnson and R. K. Ingham, Chemical Reviews, 1956, **56**, 219–269.

4   E. Bosch, M. Moreno, J. M. Lluch and J. Bertrán, The Journal of Chemical Physics, 1990, **93**, 5685–5692.

5   E. Bosch, M. Moreno and J. M. Lluch, Canadian Journal of Chemistry, 1992, **70**, 100–106.

6   A. Fernández-Ramos, J. Rodríguez-Otero and M. A. Ríos, The Journal of Physical Chemistry A, 1998, **102**, 2954–2961.

7   T. N. Truong and J. A. McCammon, Journal of the American Chemical Society, 1991, **113**, 7504–7508.

8   R. E. Continetti, International Reviews in Physical Chemistry, 1998, **17**, 227–260.

9   J. A. Gibbard, A. J. Shin, E. Castracane and R. E. Continetti, Review of Scientific Instruments, 2018, **89**, 123304.

10   Z. Lu and R. E. Continetti, The Journal of Physical Chemistry A, 2004, **108**, 9962–9969.

11   G. A. Pino, R. A. Jara-Toro, J. P. Aranguren-Abrate, C. Dedonder-Lardeux and C. Jouvet, Phys. Chem. Chem. Phys., 2019, **21**, 1797–1804.

12   M. R. Blomberg and P. E. Siegbahn, Biochimica et Biophysica Acta (BBA) - Bioenergetics, 2006, **1757**, 969 – 980.

13   H. Ishikita and K. Saito, Journal of The Royal Society Interface, 2014, **11**, 20130518.

14   A. Buonaugurio, J. Graham, A. Buytendyk, K. H. Bowen, M. R.

Ryder, Z. G. Keolopile, M. Haranczyk and M. Gutowski, The Journal of Chemical Physics, 2014, **140**, 221103.

15 H.-K. Woo, X.-B. Wang, K.-C. Lau and L.-S. Wang, The Journal of Physical Chemistry A, 2006, **110**, 7801–7805.

16 X.-B. Wang, H.-K. Woo, B. Kiran and L.-S. Wang, Angewandte Chemie International Edition, 2005, **44**, 4968–4972.

17 X.-B. Wang, X. Yang, J. B. Nicholas and L.-S. Wang, Science, 2001, **294**, 1322–1325.

18 X.-B. Wang, X. Yang, J. B. Nicholas and L.-S. Wang, The Journal of Chemical Physics, 2003, **119**, 3631–3640.

19 X.-P. Xing, X.-B. Wang and L.-S. Wang, Phys. Rev. Lett., 2008, **101**, 083003.

20 X.-B. Wang, C.-F. Ding and L.-S. Wang, Phys. Rev. Lett., 1998, **81**, 3351–3354.

21 M. Ravi Kumar, S. Prabhakar, V. Nagaveni and M. Vairamani, Rapid Communications in Mass Spectrometry, 2005, **19**, 1053–1057.

22 J. E. Bartmess, NIST Chemistry WebBook, NIST Standard Reference Database Number 69.

23 C. J. Johnson, M. E. Harding, B. L. J. Poad, J. F. Stanton and R. E. Continetti, Journal of the American Chemical Society, 2011, **133**, 19606–19609.

24 Z. Lu, Q. Hu, J. E. Oakman and R. E. Continetti, The Journal of Chemical Physics, 2007, **126**, 194305.

25 M. J. Dewar and Y.-J. Zheng, Journal of Molecular Structure: THEOCHEM, 1990, **209**, 157 – 162.

26 O. Kroutil, B. Minofar and M. Kabeláč, Journal of Molecular Modeling, 2016, **22**, 210.

27 M. J. Frisch, G. W. Trucks, H. B. Schlegel, G. E. Scuseria, M. A. Robb, J. R. Cheeseman, G. Scalmani, V. Barone, G. A. Petersson, H. Nakatsuji, X. Li, M. Caricato, A. V. Marenich, J. Bloino, B. G. Janesko, R. Gomperts, B. Mennucci, H. P. Hratchian, J. V. Ortiz, A. F. Izmaylov, J. L. Sonnenberg, D. Williams-Young, F. Ding, F. Lipparini, F. Egidi, J. Goings, B. Peng, A. Petrone, T. Henderson, D. Ranasinghe, V. G. Zakrzewski, J. Gao, N. Rega, G. Zheng, W. Liang, M. Hada, M. Ehara, K. Toyota, R. Fukuda, J. Hasegawa, M. Ishida, T. Nakajima, Y. Honda, O. Kitao, H. Nakai, T. Vreven, K. Throssell, J. A. Montgomery, Jr., J. E. Peralta, F. Ogliaro, M. J. Bearpark, J. J. Heyd, E. N. Brothers, K. N. Kudin, V. N. Staroverov, T. A. Keith, R. Kobayashi, J. Normand, K. Raghavachari, A. P. Rendell, J. C. Burant, S. S. Iyengar, J. Tomasi, M. Cossi, J. M. Millam, M. Klene, C. Adamo, R. Cammi, J. W. Ochterski, R. L. Martin, K. Morokuma, O. Farkas, J. B. Foresman and D. J. Fox, Gaussian 16 Revision C.01, 2016.

28 T. G. Clements and R. E. Continetti, The Journal of Chemical Physics, 2001, **115**, 5345–5348.

29 A. W. Ray, B. B. Shen, B. L. Poad and R. E. Continetti, Chemical Physics Letters, 2014, **592**, 30 – 35.

30 C. J. Johnson, R. Otto and R. E. Continetti, Phys. Chem. Chem. Phys., 2014, **16**, 19091–19105.

31 E. Hendell and U. Even, Review of Scientific Instruments, 1995, **66**, 3901–3902.

32 D. P. de Bruijn and J. Los, Review of Scientific Instruments, 1982, **53**, 1020–1026.

33 X. Xie and J. D. Simon, Optics Communications, 1989, **69**, 303 – 307.

34 A. T. J. B. Eppink and D. H. Parker, Review of Scientific Instruments, 1997, **68**, 3477–3484.

35 E. Fermi, Zeitschrift für Physik, 1931, **71**, 250–259.

36 X.-B. Wang, H.-K. Woo, B. Kiran and L.-S. Wang, Angewandte Chemie International Edition, **44**, 4968–4972.

37 R. J. Le Roy, R. G. Macdonald and G. Burns, The Journal of Chemical Physics, 1976, **65**, 1485–1500.

38 R. J. Le Roy, Computer Physics Communications, 1989, **52**, 383 – 395.